Desalination and Water Treatment
www.deswater.com
doi: 10.5004/dwt.2019.24008

152 (2019) 351–365
June

Kinetic and thermodynamic investigation on the adsorption of hexavalent chromium pollution by Fe_3O_4/AC/TiO_2 nanotubes as a novel ternary magnetic nanocomposite

Seyed Ghorban Hosseini[a,*], Javad Vahabzadeh Pasikhani[b]

[a]*Department of Chemistry, Malek Ashtar University of Technology, P.O. Box 16765-3454, Tehran, Iran, email: hoseinitol@yahoo.com*
[b]*Fouman Faculty of Engineering, College of Engineering, University of Tehran, P.O. Box 43515-1155, Fouman 43516-66456, Iran*

Received 13 September 2018; Accepted 20 February 2019

ABSTRACT

The ternary nanocomposites of TiO_2 nanotubes and magnetic activated carbon (TNTs/MAC) as a potent nanoadsorbent were fabricated for the Cr(VI) removal from wastewater. The TNTs/MAC was prepared by a hydrothermal method. The nanoadsorbents were characterized by field-emission scanning electron microscope, X-ray diffraction, energy dispersive spectrometry, Fourier transform infrared analysis and Brunauer–Emmet–Teller analysis, respectively. To investigate the adsorption kinetics and isotherm parameters, batch adsorption experiments were carried out as a function of solution pH, adsorbent dosage, initial Cr(VI) concentration, contact time, and adsorption temperature. The results demonstrated that TNTs/MAC with the highest surface area (307.87 $m^2\ g^{-1}$) has adsorption capacity of 20 mg g^{-1}. In acidic solution, the adsorption capacity of Cr(VI) onto TNTs/MAC was 1.5 times more than onto pure TNTs. The kinetic results revealed that Cr(VI) removal followed pseudo-second-order model with a correlation coefficient greater than 0.99, and adsorption isotherms were found to fit well with Langmuir model equations (R^2 = 0.995). In addition, the intra-particle diffusion kinetics implied that the adsorption rate was controlled by both boundary layer and intra-particle diffusion. Furthermore, thermodynamic evaluation indicated the adsorption of Cr(VI) was spontaneous and exothermic. Moreover, the thermodynamic variables showed that the adsorption nature of Cr(VI) onto TNTs/MAC is classified as physisorption, which was further confirmed by the Dubinin–Radushkevich model.

Keywords: TiO_2 nanotubes; Magnetic activated carbon; Ternary nanoadsorbents; Batch adsorption; Hexavalent chromium

1. Introduction

Nowadays heavy metals are among the most important pollutants in wastewater, and are becoming a major environmental issue at the global level [1]. Chromium, as an influential heavy metal, has been the concern of the world for many years for its high toxicity, carcinogenicity teratogenicity and mutagenicity to both humans and animals [2]. In natural environments, chromium possesses two oxidation states: trivalent Cr(III) and hexavalent Cr(VI) [3]. In fact, Cr(III) is a vital element in humans and is a proportionately inert genotoxic agent [4]. The public health attention of chromium is mainly related to Cr(VI) compounds, which they are highly mobile anions, water soluble, and can attack the human organs through the respiratory duct, digestive system and mucous membrane [5]. Therefore, it is necessary to removal Cr(VI) compounds from wastewater. According to the World Health Organization and the United States Environmental Protection Agency, the maximum permissible limit of Cr(VI) in drinking water is 50 ppb [6]. During the last decade, many different technologies have been developed to remove Cr(VI) from wastewater, such as electrochemical precipitation, membrane separation, ion-exchange, and so on [7–10]. However, most of these methods suffer from

* Corresponding author.

drawbacks that limit their application in industry, such as high operating costs, production of secondary pollutants, and increased waste sludge formation [11]. Adsorption of Cr(VI) is considered to be one of the most promising technologies for its simplicity in operation, cost-efficiency, and absence of secondary pollution [12,13]. The efficiency of adsorption process strongly depends on the choice of adsorbent. Hence, lots of adsorbents have been applied to eliminate Cr(VI) from wastewater, including activated carbon, carbon nanotubes, biosorbent, biopolymer, alumina, and zeolite [14–19]. Among these adsorbents, activated carbon is not only very cheap available material, but also has a porous structure which contains the high specific surface area and an excellent adsorption capacity [20,21]. However, several problems such as non-selectivity, unknown stability, very difficult regeneration and slow adsorption rate are associated with their use [13,22].

Several papers published within the last years indicate that by incorporation of magnetite nanoparticles into activated carbon to form magnetic activated carbon (MAC) nanocomposite adsorption rate of Cr(VI) could be enhanced [23,24]. This is due to the significant physicochemical properties of magnetite nanoparticles such as small particle sizes, large surface area, high adsorption capacity and charge on its surface [25]. Additional advantages of magnetite nanoparticles as nanoadsorbents is that they have fast rate of pollutant elimination, easily separated by high gradient magnetic field and reuse of adsorbent along with significant reduction of sludge volume [26]. Furthermore, unpaired electrons in the 3d shell of magnetite ions can act as reducing agents to chemical reduction of Cr(VI) followed by precipitation in that Cr(VI) is converted to Cr(III) [27]. However, the hydrophobic surface of magnetite nanoparticles restricts its dispersion into aqueous systems and affects their adsorption capacity and selectivity as a consequence of limit chemical and physical reactivity toward interaction with other species [3]. Hence, it is necessary to find out newly favorable adsorbent for removal of Cr(VI) from wastewater.

In order to overcome these problems, surface modifications of MAC nanocomposite by TiO_2 nanomaterials can be a good solution. This is because TiO_2 nanomaterials have many suitable advantages such as superhydrophilic surface, unique chemical, and physical properties, exceptional stability, low cost, nontoxicity, and abundance [28,29]. It should be noted that an ideal adsorbent must have a high surface area, uniformly accessible pores, and physical and/or chemical stability [26]. In comparison with different TiO_2 nanostructures, TiO_2 nanotubes (TNTs) synthesized via hydrothermal method, possess many benefits such as simple synthesis, providing the high specific surface area, good sedimentation property, and facilitate the transport of reagents to reactive sites [30–32]. Thus, TNTs coated onto MAC can be a promising nanoadsorbent to remove Cr(VI) ions from wastewater.

To the best of our knowledge, the application of TNTs-coated MAC for removal of Cr(VI) from the aqueous environment has not been reported so far. Thereby, in this study, a novel TNTs/MAC nanocomposite was fabricated for removal of Cr(VI) from the wastewater. Also, the effects of pH value, adsorbent dosage, initial Cr(VI) concentration, and contact time were examined. Moreover, to investigate the adsorption kinetics, isotherms and thermodynamics, the experimental data were fitted with different models.

2. Experimental

2.1. Chemicals and materials

All chemicals in the analytical reagent grade were used as received without further purification, and all solutions throughout experiments were prepared with deionized water. Sodium hydroxide pellets (NaOH), hydrochloric acid (HCl), iron(III) chloride hexahydrate ($FeCl_3.6H_2O$), and iron(ii) sulfate heptahydrate ($FeSO_4.7H_2O$) were all Merck chemicals (Darmstadt, Germany). The commercial TiO_2 powder (P25, Evonik, Germany) was used for making the TNTs. High-purity potassium dichromate ($K_2Cr_2O_7$, >99% purity) was utilized as a probe molecule for adsorption tests.

2.2. Synthesis of the nanoadsorbents

2.2.1. Fabrication TNTs

In this research, TNTs were fabricated by the hydrothermal method. The precursor materials for TNTs preparation included a commercial TiO_2 powder (P25, Evonik, Germany) and sodium hydroxide pellets, and these chemicals were used without further purification. Generally, 2 g of commercial TiO_2 powder was dispersed into 100 mL of 10 M NaOH solution and stirred for 30 min at room temperature to form a suspension. Then, this suspension solution was transferred into a Teflon vessel reactor and remained in an autoclave to be heated at 423.15 K for 24 h. After cooling down to room temperature, the resulting white precipitates were separated from the reaction solution, followed by thorough washing with diluted HCl solution (0.1 M) and distilled water repeatedly until the pH of the solution reached near neutral. Finally, the hydrothermal products separated from the washing solution by filtration, dried at 80°C in an oven. The as-synthesized TNTs were then calcined at 673.15 K in air for 2 h.

2.2.2. Preparation of MAC

The MAC was prepared via a modified co-precipitation method as reported by Ma et al. [33]. In brief, $FeCl_3.6H_2O$ (9.45 g, 35 mmol) and $FeSO_4.7H_2O$ (9.75 g, 35 mmol) at a mole ratio of 1:1 were dissolved in deionized water and followed by the addition of 8.25 g activated carbon (AC). The mixture was then subject to vigorous stirring under the anoxic condition at ambient temperature for 1 h. Afterward, the pH was adjusted to 10 by adding 2.5 M NaOH into the iron salt solution. The formed solution was stirred and maintained at 100°C with a thermostatic water bath for 2 h. Finally, the synthesized MAC was separated by a magnet, and the particles were washed with distilled deionized water many times to obtain a neutral pH.

2.2.3. Synthesis of TNTs/MAC

In this research, the hydrothermal method has been employed for the preparation of TNTs-MAC nanocomposite (TNTs/MAC) using TNTs and MAC as raw materials. In

a typical synthesis, MAC was first dispersed in H_2O by ultrasonic treatment for 1 h to yield a homogenized solution. Subsequently, TNTs were added into the MAC and the solution was homogenized. After stirring for another 1 h, the obtained homogeneous suspension was transferred to a Teflon-lined autoclave and was subjected to hydrothermal treatment at 423.15 K for 6 h. The resultant composite was collected by centrifugation, repeatedly washed with water, and dried at 353.15 K, respectively. Moreover, the TNTs-AC) nanocomposite was also prepared according to the above procedure which AC was used as raw materials instead of MAC.

2.3. Catalysts characterization

The as-synthesized nanoadsorbents were analyzed through X-ray diffraction (XRD) experiments, which was performed on an X-ray diffractometer (Philips X'Pert Pro X-ray, Germany) using Cu Kα radiation (λ = 1.5406 Å) in the 2θ range of 10°–80° to identify the crystalline phase. The surface morphologies and elements present in the as-prepared nanoadsorbents were examined using a field-emission scanning electron microscope (FESEM, TESCAN MIRA3-XMU, Czech Republic) with an energy dispersive spectrometry (EDS) detector for spectrometry. To determine the functional groups available in the as-synthesized nanoadsorbents, the Fourier transform infrared analysis (FTIR; Bruker alpha-2000, USA) was performed over a wavenumber range of 500–4,000 cm^{-1}. The Brunauer–Emmet–Teller (BET) analysis of the nanoadsorbents was investigated using a micrometer ASAP 2000 (USA). The BET method measures the specific surface area and the pore volume. Besides, the average pore size and its distribution were estimated from adsorption isotherms by Barrett–Joyner–Halenda analysis. The rationale of this technique is based on multiple points of nitrogen gas isothermal adsorption–desorption. Furthermore, the magnetic properties (M-H curve) were collected at ambient temperature by using a vibrating sample magnetometer (VSM).

2.4. Study on the point of zero charge

In the PZC (pH) determination, 0.01 M NaCl was prepared, and its pH was adjusted in the range of 2–12 by adding 0.01 M NaOH or HCl. Then, 50 mL of 0.01 M NaCl each was put in a conical flask, and then 0.1 g of prepared samples was added to these solutions. These flasks were kept for 72 h, and the final pH of the solution was measured by using a pH meter. Graphs were then plotted for pH_{final} vs. $pH_{initial}$.

2.5. Adsorption experiments

The adsorption characteristics of the as-prepared nanoadsorbents were evaluated by the elimination of hexavalent chromium from wastewater in the batch experiments. In this research, the adsorption behavior of Cr(VI) onto TNTs, TNTs/AC, and TNTs/MAC nanocomposites was investigated as a function of important parameters including solution pH, adsorbent dosage, initial Cr(VI) concentration, contact time, and adsorption temperature, respectively. A stock solution of 1,000 ppm Cr(VI) was prepared by dissolving a certain amount of analytical grade potassium dichromate ($K_2Cr_2O_7$, >99% purity) in deionized water, and the other solutions were prepared by dilution. To investigate the effect of pH, adsorption tests were carried out at different pH levels in the range of 2–12 with 0.01 g of TNTs, TNTs/AC, and TNTs/MAC nanocomposites by setting the initial Cr(VI) concentrations at 10 ppm. In these experiments, NaOH (0.1 M) and HCl (0.1 M) were employed to regulate the pH level. For determination of optimal nanoadsorbent dosage, tests were done at the different nanoadsorbent amount in the range from 0.01 to 0.5 g at optimal pH in Cr(VI) solution with 10 ppm initial concentrations. Adsorption isotherm studies were conducted with initial Cr(VI) concentrations ranging in 10–50 ppm at constant temperature and optimal solution pH. Adsorption kinetic experiments were performed to investigate the effect of contact time and evaluate the kinetic properties. At a definite time interval, the solutions were collected and analyzed for residual Cr(VI) ion concentration. The adsorption capacities at specific times (q_t, mg g^{-1}) and equilibrium (q_e, mg g^{-1}) were calculated using the following equations [9,18]:

$$q_t = \frac{C_0 - C_t}{m} \times V \tag{1}$$

$$q_e = \frac{C_0 - C_e}{m} \times V \tag{2}$$

where C_0, C_e, and C_t are the concentration of Cr(VI) (ppm) at the initial, at equilibrium and at t time, respectively. V is the volume of the Cr(VI) solution (L), and m is the mass of nanoadsorbents (g). The Cr concentration before and after adsorption was measured three times using a UV–vis/NIR spectrophotometer. Also, the chromium removal percent (%R) was estimated as follows [6]:

$$\%R = \left(1 - \frac{C_t}{C_0}\right) \times 100 \tag{3}$$

Furthermore, to estimate the feasibility of the process of Cr(VI) ions adsorption onto nanoadsorbents and calculate the thermodynamic parameters, the adsorption studies were carried out at different temperatures in the range of 298.15–328.15 K.

3. Results and discussion

3.1. FESEM and EDS

Figs. 1(a)–(c) show the FESEM images of TNTs, TNTs/AC, and TNTs/MAC nanocomposites, respectively. According to Fig. 1(a), the TiO_2 samples that prepared by hydrothermal procedure exhibit smooth surface and nanotubular morphology with the length of several hundred nanometers. After modification of TNTs with AC and MAC nanoparticles, changes were observed on the surface of TNTs. As shown in Figs. 1(b) and (c), the porous activated carbon and the very fine spherical shape Fe_3O_4 nanoparticles were effectively attached on the surface of TNTs, which indicates the relatively high interfacial adhesion between the

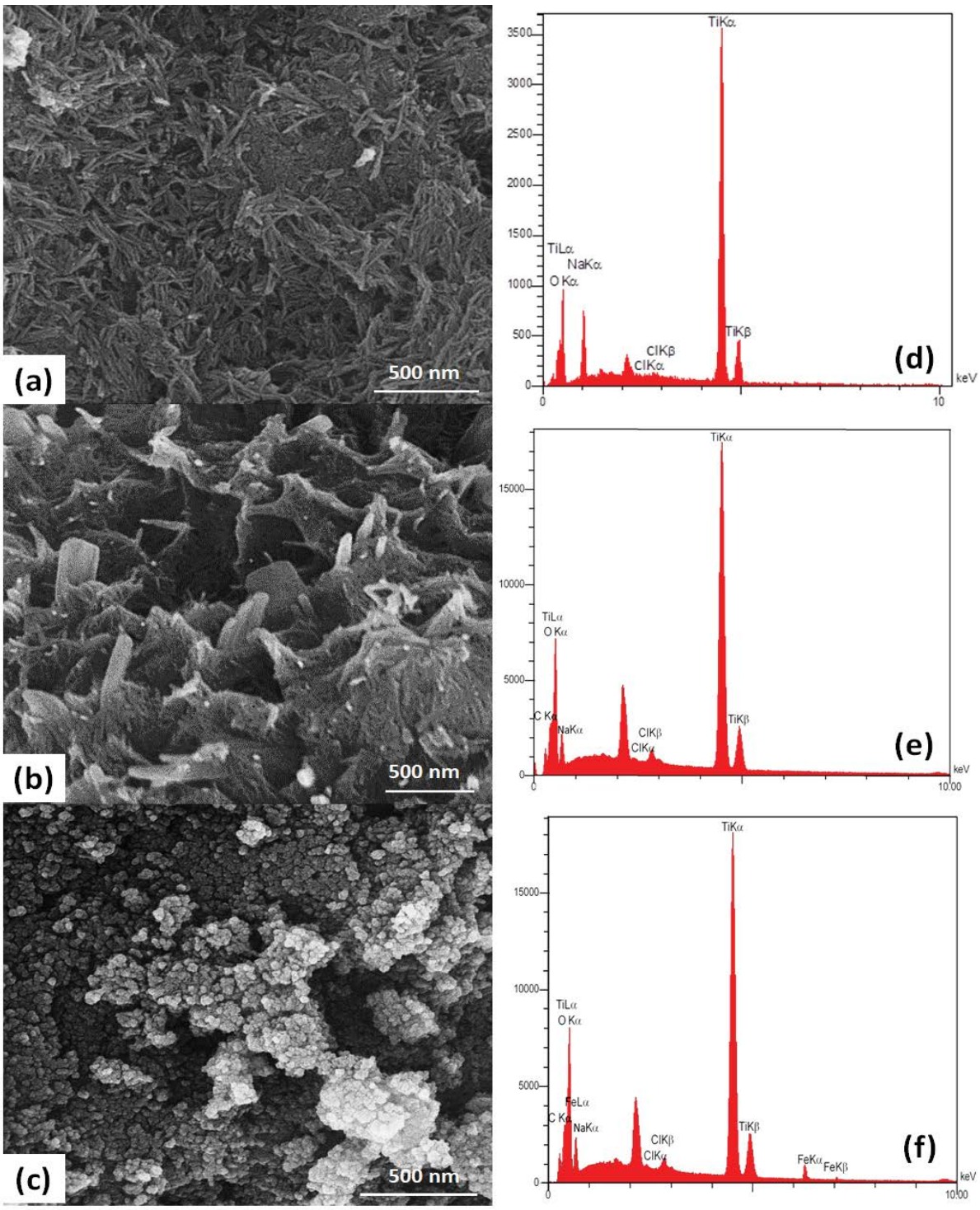

Fig. 1. FESEM images of (a) TNTs, (b) TNTs/AC, and (c) TNTs/MAC, and EDS spectra of (d) TNTs, (e) TNTs/AC, and (f) TNTs/MAC.

TNTs, AC, and Fe_3O_4 nanoparticles. The relative elemental compositions of nanoadsorbents obtained from EDS analysis are presented in Figs. 1(d)–(f). Based on these images, the presence of carbon in TNTs/AC and TNTs/MAC was further confirmed by EDS analysis. It is clear from Fig. 1(f) that the peaks of iron have appeared in the spectrum. In sum up, the EDS analysis revealed that the TNTs/MAC as ternary nanocomposites mainly consisted of Ti, O, Na, Cl, C, and Fe atoms.

3.2. XRD

The XRD patterns of the TNTs, TNTs/AC, and TNTs/MAC nanocomposites are shown in Fig. 2. The patterns

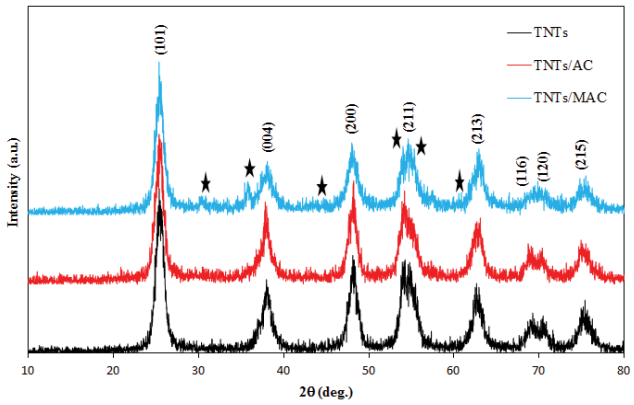

Fig. 2. XRD pattern of the as-synthesized TNTs, TNTs/AC, and TNTs/MAC.

show the presence of TiO_2 anatase (101) as the main phase at 2θ of 25.3°. The diffraction peaks which were observed at 37.9°, 48.1°, 53.8°, 55.2°, 62.2°, 68.8°, 70.02°, and 75.09° represent other nanocrystalline of the anatase phase that can be indexed to the (004), (200), (105), (211), (213), (116), (220), and (215), respectively [34,35]. When XRD patterns of the TNTs/AC were compared with TNTs, the dope of AC does not lead to the change in the numbers and the positions of diffraction peaks and it keeps the anatase crystalline phase also. As illustrated in Fig. 2, the iron atoms significantly affected on intensity and numbers of XRD patterns of TNTs. It could be seen that dominant diffraction peaks (showed with an asterisk) at 2θ = 30.2°, 35.6°, 43.5°, 54.7°, 56.9°, and 62.5° can be, respectively, indexed to (220), (311), (400), (422), (511), and (440) planes of magnetite nanoparticles. The results are in a good agreement with the cubic spinel structured of the Fe_3O_4 that reported by JCPDS card number 19-0629 [2].

3.3. FTIR

The surface functional groups of the as-prepared nanoadsorbent were characterized by FTIR spectrum and are presented in Fig. 3. In FTIR spectra, the vibration near 583 cm^{-1} is indexed to the characterized vibrations of Ti–O and Fe–O. Moreover, the vibration at 1,389 cm^{-1} is ascribed

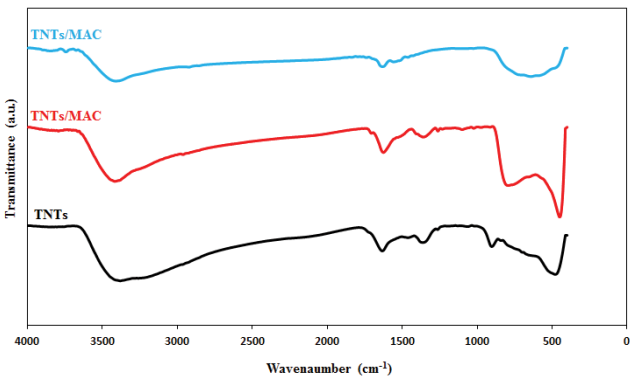

Fig. 3. FTIR spectra of the as-synthesized TNTs, TNTs/AC, and TNTs/MAC.

to the O–H bond vibration of Ti–OH on the surface of particles. The peaks observed at around 3,420 and 2,962 cm^{-1} are attributed to the Ti–OH bond [36]. The OH bending vibration of chemisorbed and/or physisorbed water molecule on the surface of the catalysts is observed near 1,630 cm^{-1} for all the samples [35]. The broad absorption peaks from 800 to 700 cm^{-1} and 490 to 433 cm^{-1} are ascribed to the asymmetric stretching, symmetric stretching, and the bending modes of Ti–O–Ti bond, respectively [37]. The peaks at 1,529, 1,593, and 1,396 cm^{-1} were corresponding to the vibration of –C–C and –C=O stretching vibrations, respectively, which came from the used precursor and solution [38]. For all photocatalysts, a small peak at around 3,780 cm^{-1} which is assigned as O–H stretching of the hydroxyl group to Ti atoms was observed [39]. The low-intensity broadband at around the 840 cm^{-1} is characteristic of the Na–O bending of the Na–O–Ti bond of sodium titanates [40]. These results confirmed that C and Fe species had been incorporated into the TNTs lattice which is well in agreement with EDS results.

3.4. BET

The structural characteristics and pore size distribution of the as-synthesized catalysts were evaluated via N_2 adsorption–desorption analyses, as shown in Fig. 4, and the corresponding pore properties are summarized in Table 1. All adsorption isotherms demonstrate similar typical type IV isotherm with an evident type-H3 hysteresis loop in the relative pressure (P/P_0) range of 0.4–1, according to the IUPAC classification [41]. This phenomenon suggests a slit-like pore geometry formed by TNTs because of their aggregation, which is typical for mesoporous materials [42]. Based on Fig. 4, it can be observed that by modification of TNTs with AC and MAC nanoparticles, the hysteresis loop of catalysts became smaller and shifted to the high relative pressure region of 0.8–1. According to Table 1, both TNTs/AC and TNTs/MAC nanoadsorbents had the highest surface area and pore volume as compared with the pure TNTs. Furthermore, the BET surface area (307.87 $m^2\ g^{-1}$) and the corresponding pore volume (0.46 $cm^3\ g^{-1}$) of TNTs/MAC are considerably largest as compared with the surface area (114.46 $m^2\ g^{-1}$) and pore volume (0.29 $cm^3\ g^{-1}$) of TNTs/AC. These results revealed that the AC and MAC augment the attractive forces of the surface in forming larger mesoporous pores. It should be noted that in adsorption process, the specific surface area of the adsorbent is important to provide enough active sites for the molecules to adsorb. Since the TNTs/MAC had the highest surface area than the two other nanoadsorbents, we expect the TNTs/MAC catalysts to exhibit a higher adsorption efficiency for removal of Cr(VI) from the wastewater.

3.5. VSM

The saturation magnetization (Ms) of the TNTs/MAC was measured to study the magnetic reaction of the magnetic nanocomposite to an external field. According to Fig. 5, the nanoadsorbent is superparamagnetic at room temperature. It is worth noting that the Ms value of the Fe_3O_4 nanoparticles is significantly higher than that of TNTs/MAC sample, which is because the Fe_3O_4 nanoparticles are covered with an anatase TNTs layer in the TNTs/MAC sample. Furthermore, no

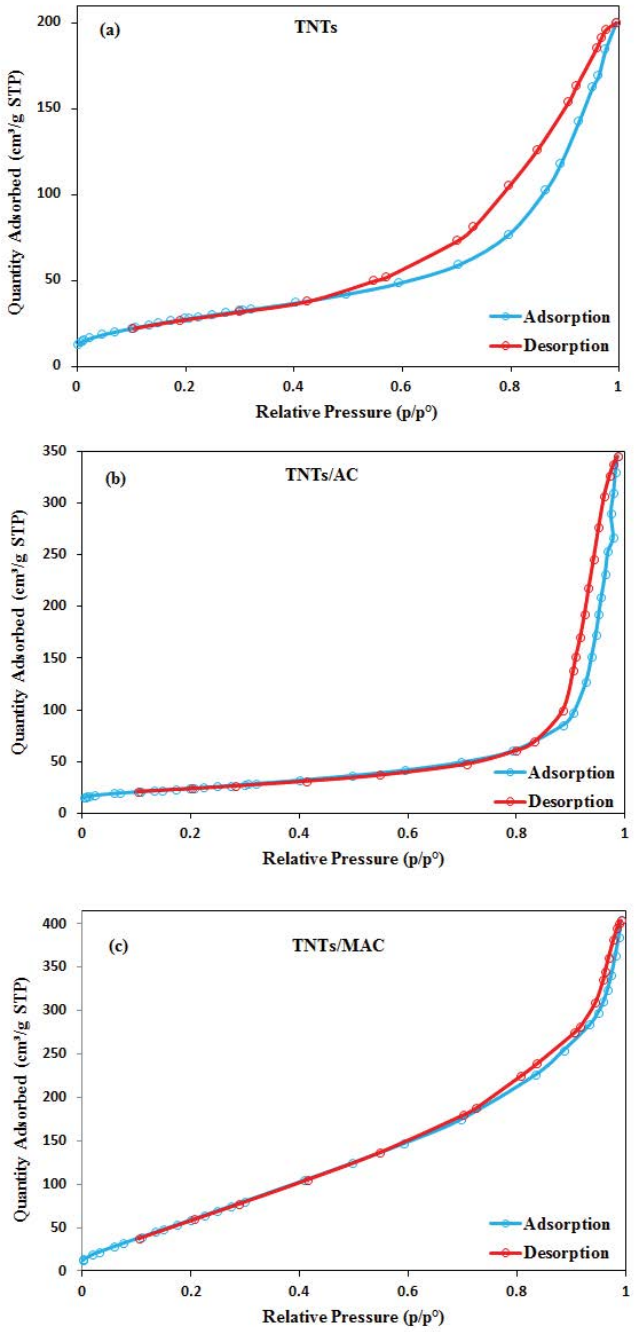

Fig. 4. N_2 adsorption–desorption isotherms for (a) TNTs, (b) TNTs/AC, and (c) TNTs/MAC.

Table 1
Surface area and total pore volume of the prepared nanoadsorbents

Adsorbent	BET surface area ($m^2\ g^{-1}$)	Pore volume ($cm^3\ g^{-1}$)
TNTs	89.54	0.25
TNTs/AC	114.46	0.29
TNTs/MAC	307.87	0.46

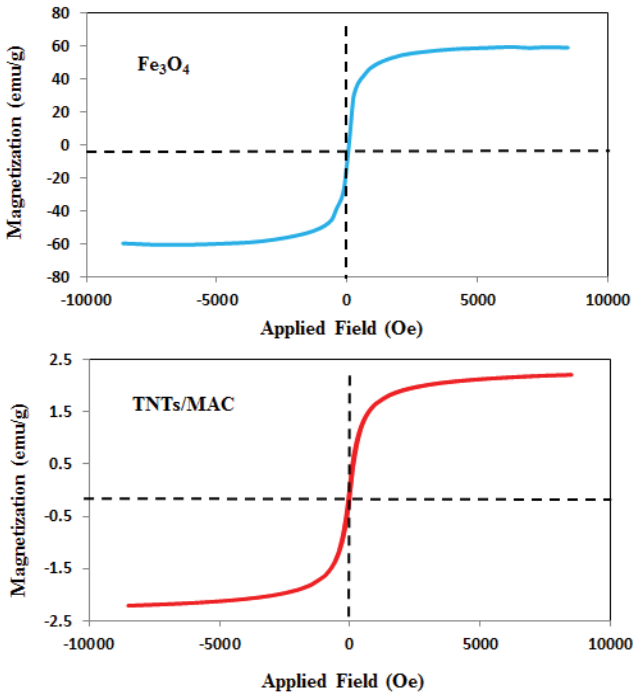

Fig. 5. Field dependence of the magnetization of TNTs/MAC measured at room temperature.

significant variation was seen in the coercivity. Such excellent magnetic properties imply a strong magnetic responsivity on the sample, enabling them to be recycled easily from solution through an external magnetic force.

3.6. Adsorption study

3.6.1. Effect of pH on the adsorption of Cr(VI)

The pH value of the pollutant solution plays a critical role in the adsorption process. This is because the solution pH affects the surface charges and the binding sites of nanoadsorbents and the interactions between them and pollutant. Fig. 6(a) depicts the removal of Cr(VI) as a function of pH by different nanoadsorbents. All nanoadsorbents showed similar adsorption trend toward Cr(VI). The adsorption of Cr(VI) was more favored in acid solution. As shown in Fig. 6(a), the maximum removal of Cr(VI) is observed at pH 2–4, and then the removal efficiency starts to decrease dramatically as the pH increases. The effect of solution pH can be explained by considering the surface charges of the nanoadsorbents and the degree of ionization of the adsorbate. In fact in aqueous solutions, Cr(VI) exists in different ionic forms at different pH conditions. H_2CrO_4 exists mainly at a solution pH below 2.0, $HCrO_4^-$ and $Cr_2O_7^{2-}$ are usually found in the pH range of 2–6, and CrO_4^{2-} is the primary form when the solution pH increases to above 7.0 [1,14]. Therefore, when the solution pH has changed, the form of the Cr(VI) ions will influence the Cr(VI) uptake capacity. The other important effective parameter for Cr(VI) adsorption is the point of zero charge (pH_{pzc}) of nanoadsorbents [15]. The graph of pH_{final} vs. $pH_{initial}$ is plotted as shown in Fig. 6(b). The intersections of the curves with the straight line are known as the endpoints of the

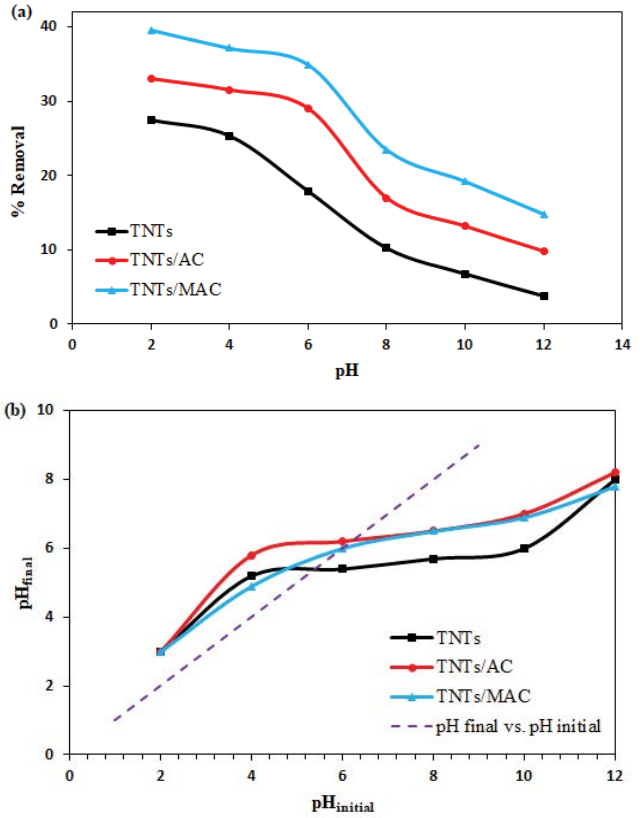

Fig. 6. (a) Effect of solution pH on Cr(VI) removal by various nanoadsorbents and (b) plot for determination of pH_{pzc} of various nanoadsorbent.

pH_{pzc}. Based on Fig. 6(b), the pH values of the PZC were 5.3, 6.3, and 6 for TNTs, TNTs/AC, and TNTs/MAC, respectively. When the solution pH value is lower than pH_{pzc} ($pH < pH_{pzc}$), the surface of nanoadsorbents are protonated and positively charged, and as a result a strong electrostatic attraction takes place between the very high positive surface charge on the nanoadsorbents and negatively charged Cr(VI) anions. However, with the increase in pH ($pH > pH_{pzc}$), the surface of nanoadsorbents becomes negatively charged, so there is a competition between OH^- ions and negatively charged ionic forms of Cr(VI) results in more eventually electrostatic repulsion.

3.6.2. Effect of nanoadsorbent dosage on Cr(VI) adsorption

Nanoadsorbent dose is an important parameter that strongly influences the adsorption process by affecting the adsorption capacity of the adsorbent. The removal percentage of Cr(VI) and adsorption capacity as a function of nanoadsorbent dosage are illustrated in Fig. 7. When the dosage of all three nanoadsorbent, namely TNTs, TNTs/AC, and TNTs/MAC, increased from 0.01 to 0.3 g, Cr(VI) removal efficiency increased remarkably. The reason is that the increase of dosage leads to an increase in the adsorbent surface area and augmenting the number of adsorption active sites available for adsorbate [43]. However, there was no remarkable increase in adsorption efficiency after adding

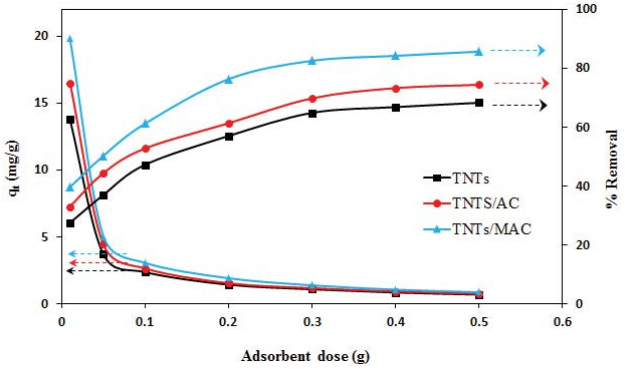

Fig. 7. Effect of nanoadsorbent dose on the Cr(VI) removal and equilibrium adsorption capacity.

further nanoadsorbents, that is, over 0.3 g. By comparing the nanoadsorbents performance at 0.3 g, it can be seen that the removal efficiency of Cr(VI) over TNTs/AC and TNTs/MAC are 1.09 and 1.25 times higher than the removal efficiency of Cr(VI) over TNTs. Moreover, for all samples, adsorption capacity decreased as dosage increased. This can be attributed to the fact that the increase of dosage leads to aggregation of nanoparticles, and then reduces adsorption sites [16]. Therefore, in the following experiments, the adsorbent dose was fixed at 0.3 g as the best nanoadsorbent dosage.

3.6.3. Effect of initial concentration and contact time on Cr(VI) adsorption

The effect of initial concentration of Cr(VI) and contact time on the adsorption capacity over TNTs, TNTs/AC, and TNTs/MAC nanoadsorbents are presented in Figs. 8(a)–(c), respectively. The initial concentration of Cr(VI) is an effective factor in the adsorption process. Experimental results revealed that the removal efficiency decreased as a function of the increase in initial concentrations of Cr(VI), for all samples. That is because the removal percentage of Cr(VI) strongly depends on the immediate relationship between the Cr(VI) molecules and the available binding sites on the adsorbent surface [18]. At low concentrations, active sites on the adsorbent surface are unoccupied, but when the initial Cr(VI) concentration increases, the active sites needed for adsorption of the Cr(VI) molecules will not be available [44]. So it is evident that the removal percentage decreases with an increase in the initial concentration of Cr(VI), as a consequence of the saturation of adsorption sites on the adsorbent surface [45]. As shown in Fig. 8, it is observed that all three nanoadsorbents followed the same changing trend, and adsorption capacity increased with the increase of Cr(VI) concentration. This may be attributed to the high driving force for mass at a high initial concentration of Cr(VI). In other words, the concentration gradient between the bulk solution and the particle surface enhances the adsorption rate [46]. Furthermore, it was found that the rate of adsorption was rapid for the first 20 min and after that it proceeded at a slower rate (20–120 min) and finally reached saturation. The maximum adsorption capacity over TNTs, TNTs/AC, and TNTs/MAC nanoadsorbents were, respectively, increased from 0.69 to 1.71 mg g^{-1}, 0.74 to 2.02 mg g^{-1} and 0.86 to 2.47 mg g^{-1}, as a function of the increase in initial concentrations of Cr(VI).

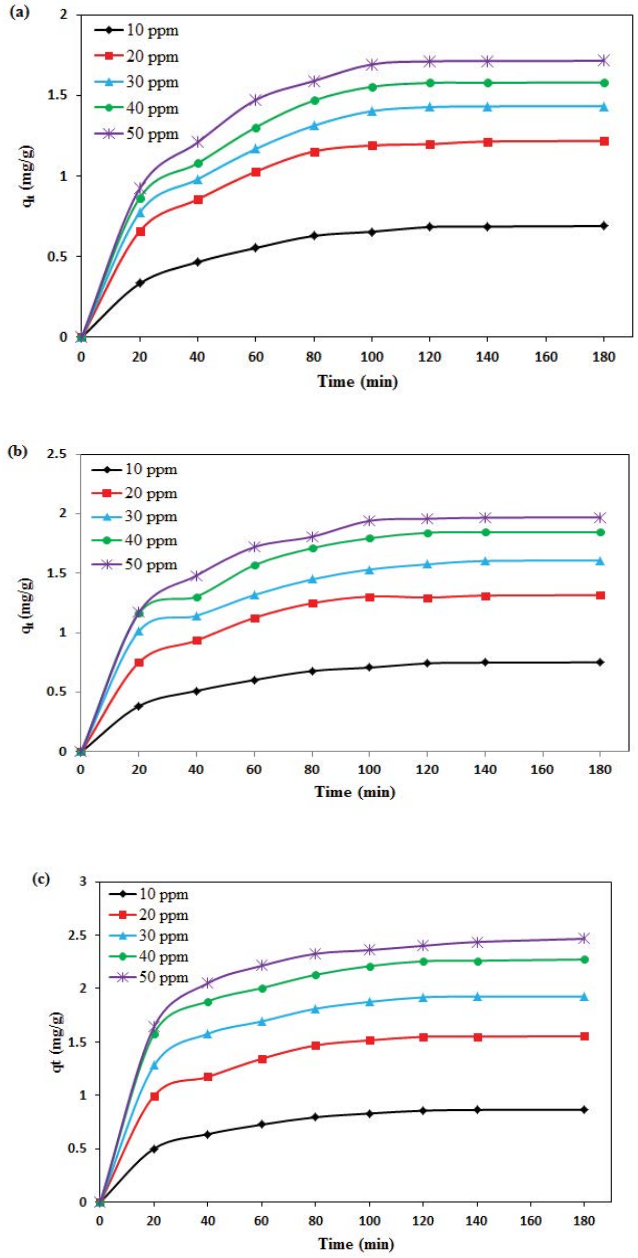

Fig. 8. Effect of contact time and initial concentration on the adsorption of Cr(VI) onto (a) TNTs, (b) TNTs/AC, and (c) TNTs/MAC.

3.6.4. Adsorption kinetics

To evaluate the adsorption kinetics, four different kinetic models, namely pseudo-first-order (Lagergren), pseudo-second-order, Elovich, and intra-particle diffusion model (Weber–Morris model), were employed to the data.

The pseudo-first-order and pseudo-second-order that are often applied as adsorption kinetic models are expressed as follows [26,27]:

Pseudo-first-order:

$$\ln\left(q_e - q_t\right) = \ln\left(q_e\right) - k_1 t \tag{4}$$

Pseudo-second-order:

$$\frac{t}{q_t} = \frac{1}{k_2 q_e^2} + \frac{t}{q_e} \tag{5}$$

where q_e (mg g^{-1}) and q_t (mg g^{-1}) are the adsorption capacities at equilibrium and at time t (min), respectively, and k_1 (min^{-1}) is the rate constant of the pseudo-first-order model and k_2 (g (mg min)$^{-1}$) is the rate constant of the pseudo-second-order model. The values of q_e, k_1, and k_2 can be calculated from the intercept and slope of the plot of $\ln(q_e - q_t)$ vs. t and the plot of (t/q) vs. t, respectively. To confirm the diffusion mechanism, the Weber–Morris model can be appropriate. The Weber–Morris equations can be defined with the below equation [3]:

Intra-particle diffusion:

$$q_t = k_{\text{dif}}\sqrt{t} + C \tag{6}$$

where k_{dif} (mg (g min)$^{-1}$) is the intra-particle diffusion rate constant and C (mg g^{-1}) is related to the thickness of the boundary layer. Elovich kinetic model is represented by another rate equation based on adsorption capacity and is expressed by the following equation [47]:

Elovich:

$$q_t = \frac{\ln(\alpha\beta)}{\beta} + \frac{\ln t}{\beta} \tag{7}$$

where α (mg (g min^2)$^{-1}$) is the initial adsorption rate of the Elovich equation, and β (mg (g min)$^{-1}$) is the desorption constant related to the extent of surface coverage and activation energy for chemical adsorption.

The results of four kinetic models over three nanoadsorbents at 50 ppm initial concentrations of Cr(VI) are presented in Figs. 9(a) and (b). Also, all kinetic parameters for different initial concentrations are listed in Table 2. The correlation coefficients (R^2) were compared to find the best and appropriate kinetic model. According to Fig. 9 and Table 2 it can be observed that for all nanoadsorbents, pseudo-second-order model is more appropriate for fitting experimental data due to the higher correlation coefficient value, compared with other kinetic models. So the pseudo-second-order model is the ideal model to describe the adsorption kinetics of Cr(VI) by three nanoadsorbents, namely TNTs, TNTs/AC, and TNTs/MAC. In fact, the pseudo-second-order model may be used to imply that the overall rate of the adsorption process is controlled by chemical adsorption (chemisorption) processes [27]. Chemisorption behavior apparently attributed to the valence forces that include the exchange or sharing of electrons between cation groups of nanoadsorbent and anion groups of adsorbate [48]. Based on Table 2, the calculated values of adsorption capacity ($q_{e(\text{cal})}$) from the pseudo-second-order model well agree with the experimental values of equilibrium capacity (q_e). However, the small difference between the theoretical and experimental values of adsorption capacity may relate to the uncertainty inherent in achieving the experimental q_e values. Furthermore, the data indicated that $q_{e(\text{cal})}$ and k_2 for the pseudo-second-order

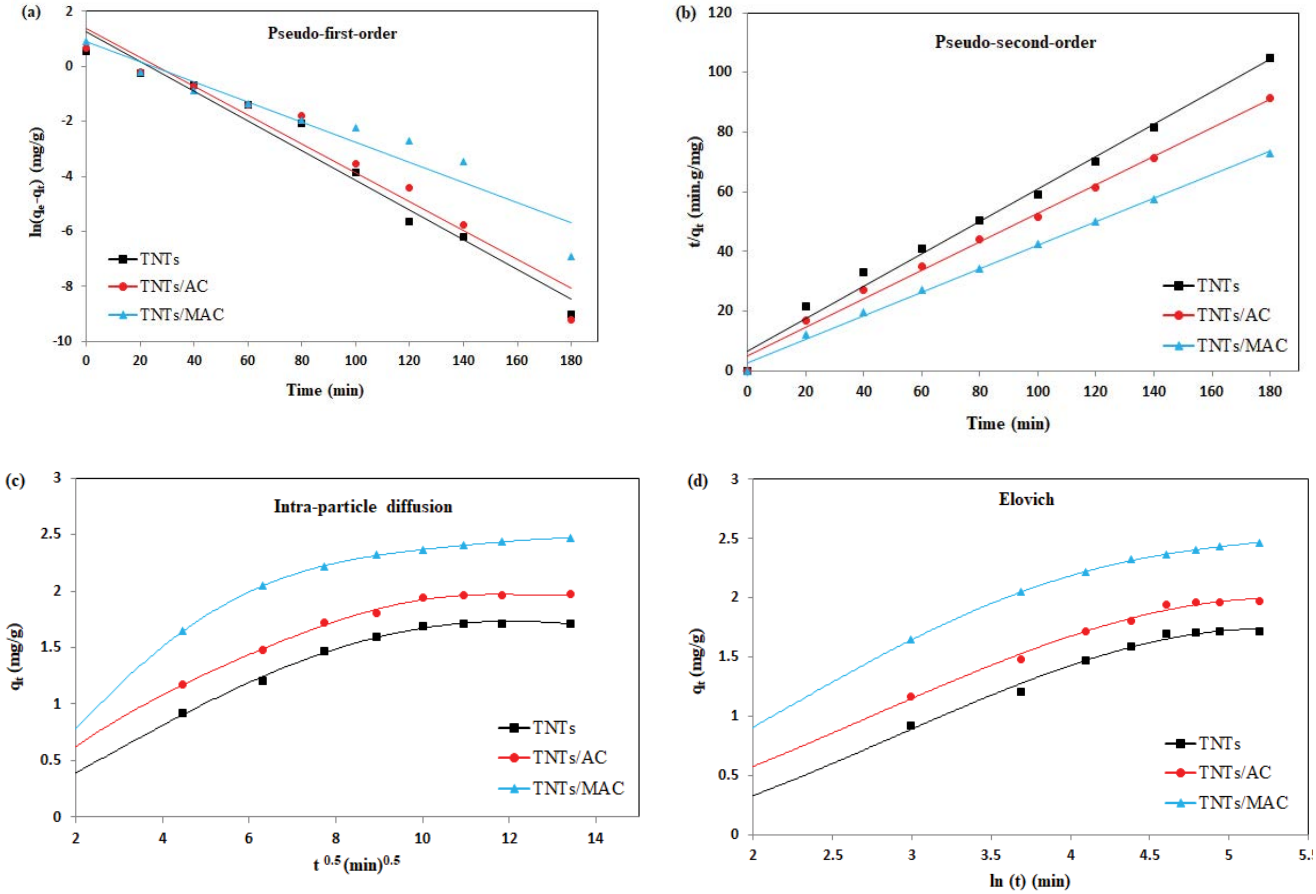

Fig. 9. Kinetic plots for Cr(VI) adsorption (a) pseudo-first-order, (b) pseudo-second-order, (c) intra-particle model, and (d) Elovich model.

model, respectively, increased and decreased as a function of the increase in initial concentrations of Cr(VI) for all nanoadsorbents. The increase in $q_{e(cal)}$ may be ascribed to decrease in mass transfer resistance of adsorbate from bulk solutions to the adsorbent surface [1]. In addition, the decrease in k_2 with increasing initial Cr(VI) concentration indicate that the time needed to reach adsorption equilibrium raised with increase in initial Cr(VI) concentration [11]. To understand the adsorption mechanism in elimination of Cr(VI) ions, it is important to determine the rate-limiting step especially when the process is fulfilled as a batch procedure [1]. It is now well established that, in the solid–liquid adsorption during the adsorption of adsorbate over a porous adsorbent, three consecutive steps were taken place as follows [2]:

- Transport of the adsorbate ions from the bulk solution to the external surface of the porous adsorbent (boundary layer diffusion).
- Permeation of the adsorbate ions into the interior of the pores of adsorbent (intra-particle diffusion).
- Adsorption of the adsorbate ions onto the cationic active sites of the adsorbent.

Generally, the third step is considered to be very fast and is not the rate-limiting step in the uptake of ionic pollutant. Thus, the adsorption kinetics can be controlled by boundary layer diffusion or intra-particle diffusion, or both of them. The intra-particle diffusion can be discussed by Weber–Morris model and is expressed as Eq. (6). If the plot of q_t vs. $t^{0.5}$ presents a linear relationship and the intercept is zero (C = 0), the adsorption rate is exclusively controlled by intra-particle diffusion. While if the plot gives more than one straight line, adsorption rate may be controlled by two or more steps, such as boundary layer and intra-particle diffusion [49]. According to Fig. 9(c) and Table 2, the intercepts (C) were not zero and the plots of q_t vs. $t^{0.5}$ involved two linear sections. So these results confirm that the adsorption mechanism of Cr(VI) onto all three nanoadsorbents is controlled by both boundary layer diffusion and intra-particle diffusion.

3.6.5. Adsorption isotherms

Adsorption isotherms are essential for the explanation of, how the adsorbate molecules distribute between the liquid and the solid phases when the adsorption process reaches an equilibrium state. Here to evaluate the equilibrium nature of adsorption, the experimental data were fitted to three models, namely Langmuir adsorption isotherm, Freundlich adsorption isotherm, and Dubinin–Radushkevich (D-R) isotherms, respectively.

Table 2
Constant parameters and correlation coefficients calculated for various adsorption kinetic models

Adsorbents	C_i^a	q_{exp}^b	Pseudo-first-order			Pseudo-second-order			Elovich			Intra-particle diffusion		
			q_e^b	k_1^c	R^2	q_e^b	k_2^c	R^2	α^d	β^d	R^2	k_{dif}^c	C^d	R^2
TNTs	10	0.689	1.417	0.046	0.94	0.751	0.083	0.98	0.065	5.721	0.96	0.041	0.209	0.88
	20	1.217	2.333	0.048	0.94	1.306	0.0610	0.99	0.170	3.623	0.94	0.064	0.473	0.85
	30	1.432	3.417	0.055	0.95	1.550	0.046	0.99	0.178	2.986	0.95	0.079	0.516	0.88
	40	1.580	3.525	0.054	0.96	1.708	0.044	0.99	0.206	2.734	0.94	0.086	0.586	0.87
	50	1.714	3.518	0.054	0.96	1.864	0.043	0.99	0.237	2.549	0.94	0.091	0.664	0.85
TNTs/AC	10	0.741	1.599	0.047	0.93	0.815	0.081	0.99	0.082	5.519	0.97	0.043	0.249	0.89
	20	1.315	2.324	0.049	0.84	1.406	0.063	0.99	0.226	3.538	0.93	0.066	0.557	0.84
	30	1.607	3.496	0.049	0.90	1.701	0.051	0.99	0.393	3.261	0.96	0.073	0.730	0.92
	40	1.846	2.602	0.045	0.96	1.960	0.047	0.99	0.452	2.796	0.94	0.085	0.856	0.88
	50	2.021	3.918	0.052	0.95	2.087	0.047	0.99	0.456	2.563	0.95	0.091	0.917	0.86
TNTs/MAC	10	0.865	1.636	0.047	0.94	0.919	0.094	0.99	0.164	5.599	0.96	0.042	0.373	0.89
	20	1.554	2.922	0.051	0.96	1.636	0.066	0.99	0.522	3.556	0.95	0.066	0.787	0.87
	30	1.927	3.378	0.052	0.95	2.008	0.065	0.99	1.179	3.242	0.95	0.072	1.090	0.86
	40	2.273	3.604	0.048	0.91	2.355	0.061	0.99	2.286	3.021	0.96	0.077	1.362	0.88
	50	2.467	2.053	0.035	0.90	2.543	0.056	0.99	2.054	2.704	0.94	0.086	1.450	0.84

[a]Unit of C_i is mg L^{-1}.
[b]Unit of q is mg g^{-1}.
[c]Units of k_1, k_2, and k_{dif} are min^{-1}, g (mg min)$^{-1}$, and mg (g min)$^{-1}$, respectively.
[d]Units of α, β, and C are mg (g min^2)$^{-1}$, mg (g min)$^{-1}$ and mg g^{-1}, respectively.

(i) Langmuir adsorption isotherm:

This model assumes the monolayer adsorption of adsorbate on nanoadsorbent without interaction between adsorbed molecules onto surface with a finite number of homogeneous sites. The non-linear and linear forms of the Langmuir isotherm model can be described as follows [26]:

$$q_e = \frac{q_{max} k_1 C_e}{1 + k_1 C_e} \tag{8}$$

$$\frac{C_e}{q_e} = \frac{1}{k_1 q_{max}} + \frac{C_e}{q_{max}} \tag{9}$$

where C_e (mg L^{-1}), q_e (mg g^{-1}), and q_{max} (mg g^{-1}) are the equilibrium concentration, the equilibrium adsorption capacity and the maximum adsorption capacity of the adsorbents, respectively. k_L is a constant related to the binding energy of the adsorption system (L mg^{-1}). In the linear form, the values of q_{max} and k_L for preferential adsorption of Cr(VI) were calculated from the slope and intercept of the linear plot of C_e/q_e vs. C_e. Also, most of the essential factor of Langmuir isotherm is the calculation of the dimensionless constant separation factor or equilibrium parameter (R_L) which can be represented as [43]:

$$R_L = \frac{1}{1 + k_L C_{int}} \tag{10}$$

where R_L is separation factor (dimensionless), k_L is Langmuir constant and C_{int} is the initial concentration of the adsorbate. The R_L value signifies whether the adsorption is unfavorable ($R_L > 1$), linear ($R_L = 1$), favorable ($0 < R_L < 1$), or irreversible ($R_L = 0$) [43].

(ii) Freundlich isotherm:

This model is an empirical relationship that describes the multilayer adsorption of an adsorbate onto a heterogeneous surface of a nanoadsorbent. This non-linear and linear isotherm models are presented by following equations [13]:

$$q_e = k_f C_e^{1/n} \tag{11}$$

$$\ln q_e = \ln k_f + \frac{1}{n} \ln C_e \tag{12}$$

where k_f and n are Freundlich constants related to the adsorption capacity and intensity, respectively. In the linear form, the slope and intercept of the linear plot of $\ln(q_e)$ vs. $\ln(C_e)$ give the value of n and k_f. Actually, n denotes the favorability of adsorption process. For $n < 1$, the adsorption is considered poor, n between a value of 1 and 2 the adsorption is defined as moderately difficult with n values between 2 and 10 is considered good adsorption [2].

(iii) Dubinin–Radushkevich (D-R) isotherms:

To investigate the equilibrium nature of adsorption, D-R isotherms are very appropriate. The non-linear and linear forms of this model are given as follows [3]:

$$q_e = q_m \exp\left(-B_{DR}\varepsilon^2\right) \quad (13)$$

$$\ln q_e = \ln q_m - B_{DR}\varepsilon^2 \quad (14)$$

where B_{DR} is the activity coefficient related to mean adsorption energy (mol^2 kJ^{-2}), and ε is the Polanyi potential, that can be calculated from the below equation [3]:

$$\varepsilon = RT\ln\left(1+\frac{1}{C_e}\right) \quad (15)$$

where R and T are the ideal gas constant (8.3145 J (mol K)$^{-1}$) and absolute temperature (K), respectively. In the linear form, the parameters q_m and B_{DR} obtained from the intercept and slope of ln(q_e) vs. ε^2. E_a is the free energy change of adsorption (kJ mol^{-1}), which is defined as the change in the free energy during transfer of one mole of ion from infinity in solution to the adsorbent surface, that it can be calculated from the below equation [1]:

$$E_a = \frac{1}{\sqrt{2B_{DR}}} \quad (16)$$

The magnitude of E_a is used to determine the type of adsorption reaction (physical or chemical). In this regard, if E_a < 8 kJ mol^{-1}, the mechanism of adsorption is physical adsorption, if 8 < E_a < 20 kJ mol^{-1} adsorption is dominated by chemical ion exchange and if E_a > 20 kJ mol^{-1}, mechanism of adsorption is chemical adsorption [16].

The linear and non-linear fits of adsorption isotherms for different nanoadsorbents are plotted in Figs. 10 and 11, respectively. The isotherm parameters and correlation coefficients (R^2) based on Langmuir model, Freundlich model, and D-R model are presented in Table 3. According to Table 3, it can be observed that by utilizing non-linear isotherms there are no problems with transformations of non-linear various isotherms equations to linear forms, and also they are in the same error structures. Based on comparison of the correlation coefficients, it can be concluded that the correlation coefficient of the Langmuir isotherm is superior to the Freundlich and D-R isotherms, indicating that the experimental data matched with the Langmuir isotherm model. Thereby, the adsorption behavior of Cr(VI) onto three nanoadsorbent, namely TNTs, TNTs/AC, and TNTs/MAC, is considered as monolayer homogeneous adsorption process. As shown in Table 3, the R_L values for TNTs, TNTs/AC, and TNTs/MAC nanoadsorbents are in the ranges of 0.094–0.341, 0.090–0.331, and 0.061–0.245, respectively. These results indicate that the adsorption of Cr(VI) ions onto TNTs, TNTs/AC, and TNTs/MAC nanoadsorbents refers to the favorable process. Meanwhile, the values of n for TNTs, TNTs/AC, and TNTs/MAC nanoadsorbents are 3.103, 2.955, and 3.093, respectively. Thus the greater values of n than one confirms that adsorption of Cr(VI) ions onto TNTs, TNTs/AC, and TNTs/MAC nanoadsorbents can be fitted to Langmuir isotherm model. The maximum adsorption capacity (q_{max}) values of Cr(VI) ions onto TNTs, TNTs/AC, and TNTs/MAC nanoadsorbents from Langmuir model were

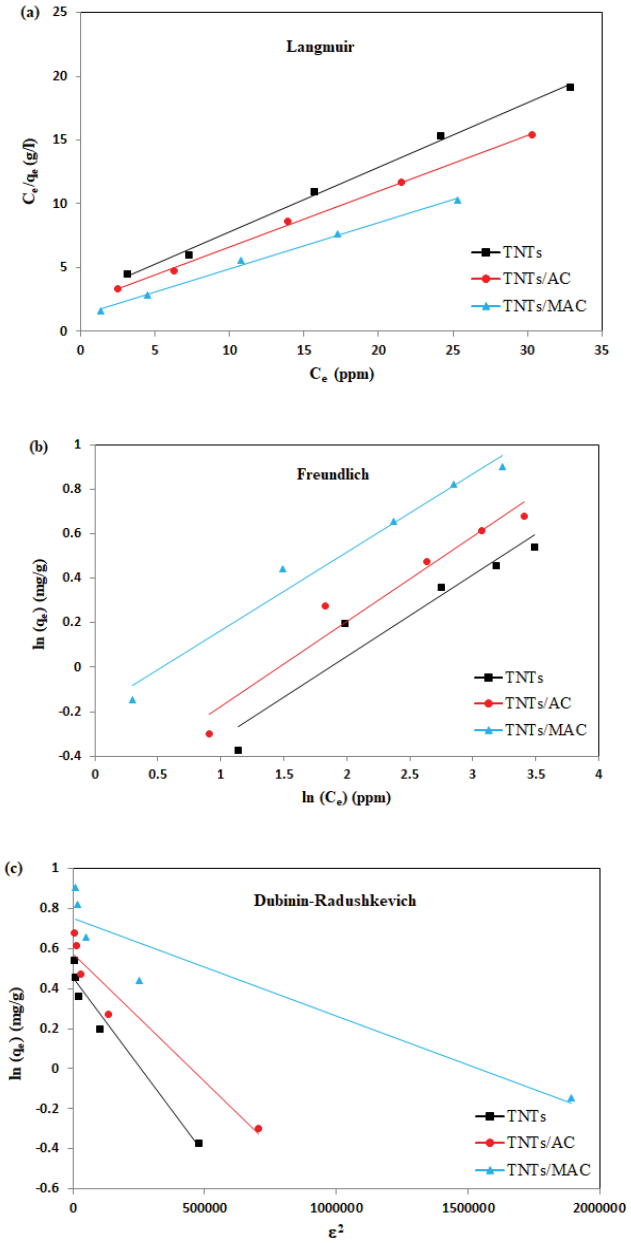

Fig. 10. Linear isotherm models of Cr(VI) onto various nanoadsorbents (a) Langmuir, (b) Freundlich, and (c) Dubinin–Radushkevich models.

1.952, 2.263, and 2.686 mg g^{-1}, respectively. These results reveal that by modification of TNTs with MAC nanoparticles, the adsorption rate of Cr(VI) can be enhanced notably. Moreover, the values of free energy (E_a) were 0.511, 0.590, and 0.941 for TNTs, TNTs/AC, and TNTs/MAC nanoadsorbents, respectively. This result suggests that the Cr(VI) adsorption onto these adsorbents is mainly physical adsorption because of the weak van der Waals forces [1].

3.6.6. Adsorption thermodynamics

In environmental engineering practice, both energy and entropy factors must be considered in order to determine

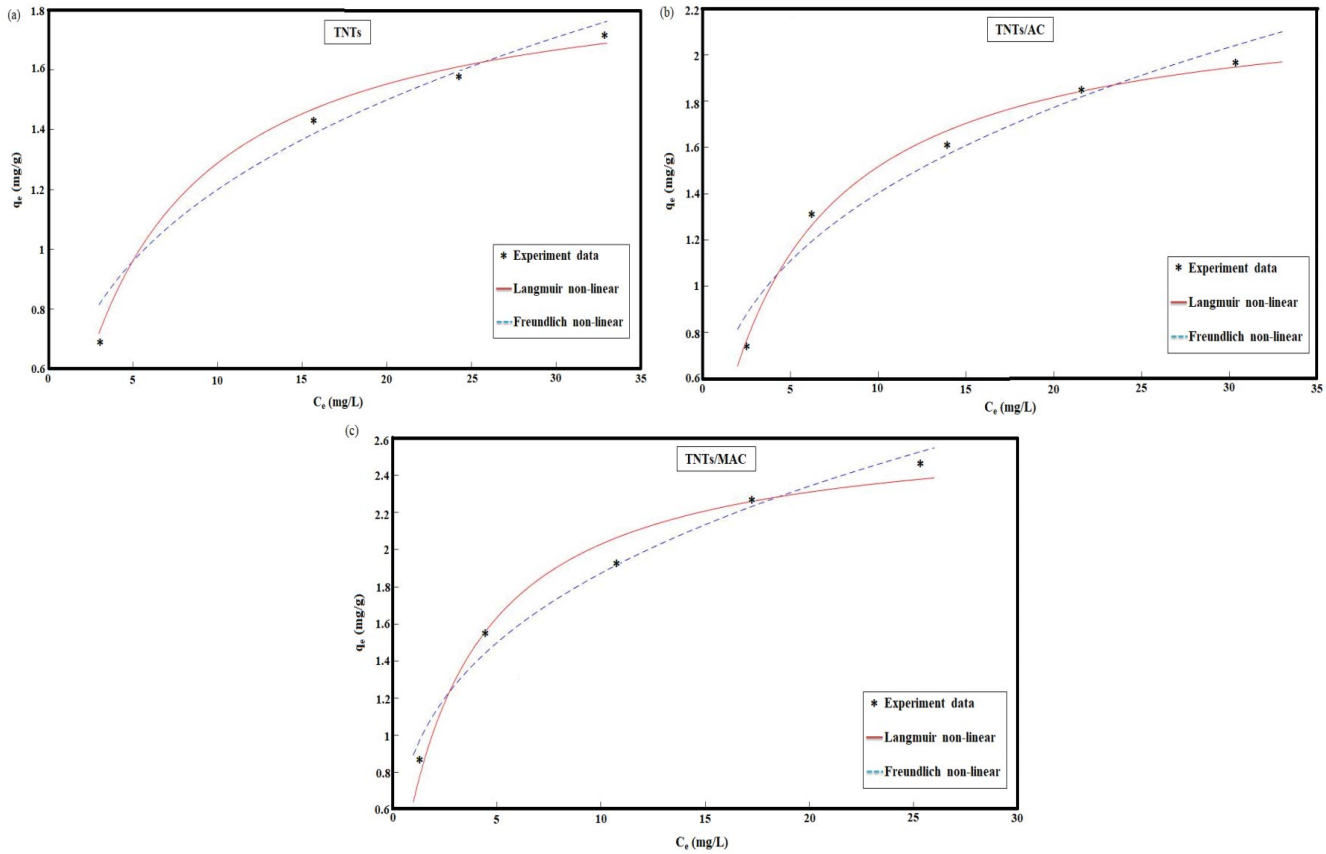

Fig. 11. Non-linear isotherm models of Cr(VI) onto various nanoadsorbents (a) TNTs, (b) TNTs/AC, and (c) TNTs/MAC.

Table 3
Isotherm parameters for the Cr(VI) removal by different nanoadsorbents

Models	Parameters	Adsorbent					
		TNTs		TNTs/AC		TNTs/MAC	
		Linear	Non-linear	Linear	Non-linear	Linear	Non-linear
Langmuir	q_m (mg g^{-1})	1.974	1.952	2.291	2.263	2.766	2.686
	k_L (L mg^{-1})	0.183	0.193	0.193	0.203	0.279	0.310
	R_L	0.098–0.353	0.094–0.341	0.094–0.341	0.090–0.331	0.067–0.264	0.061–0.245
	R^2	0.997	0.984	0.998	0.992	0.995	0.983
Freundlich	k_f (mg g^{-1})	0.505	0.571	0.574	0.643	0.828	0.890
	n	2.729	3.103	2.627	2.955	2.834	3.093
	R^2	0.925	0.937	0.957	0.959	0.976	0.980
D-R	q_m (mg g^{-1})	1.576	1.596	1.776	1.812	2.120	2.172
	B_{DR} (mol^2 kJ^{-2})	2E-6	1.916 E-6	1E-6	1.437 E-6	5E-7	5.65 E-7
	E_a (kJ mol^{-1})	0.5	0.511	0.71	0.590	1	0.941
	R^2	0.992	0.940	0.992	0.906	0.90	0.835

whether adsorption process is spontaneous or not and whether adsorption process is exothermic or endothermic. The thermodynamic parameters of standard Gibb's fre e energy change ($\Delta G°$), standard enthalpy change ($\Delta H°$), and standard entropy change ($\Delta S°$), for the adsorption processes are calculated using the following equations [26]:

$$\Delta G^{\circ} = -RT \ln k_{dc} \quad (17)$$

$$k_{dc} = \frac{q_e}{C_e} \tag{18}$$

$$\ln k_{dc} = \frac{\Delta S^o}{R} - \frac{\Delta H^o}{RT} \tag{19}$$

where k_{dc} is the thermodynamic equilibrium constant, R is the universal gas constant (8.314 J (mol K)$^{-1}$), and T is the absolute temperature (K). The values of $\Delta H°$ and $\Delta S°$ are calculated from the slope and intercept of the line relationship of the plot of ln (k_{dc}) vs. 1/T as displayed in Fig. 12. The thermodynamic variables are estimated from experimental data under different temperatures and the results are presented in Table 4. The negative values of $\Delta G°$ confirm the feasibility of the process and the spontaneous nature of sorption with a high preference for Cr(VI) to adsorb onto TNTs, TNTs/AC, and TNTs/MAC nanoadsorbents, respectively. The negative values of $\Delta H°$ indicate an exothermic nature of the adsorption process. So these results imply that the adsorption process is energetically stable and an improvement in adsorption performance can be obtained at lower temperatures. Also, the positive values of $\Delta S°$ suggest the increase in randomness at the solid/solution interface. Furthermore, the values of $\Delta G°$ and $\Delta H°$ demonstrate the nature of Cr(VI) ions sorption onto nanoadsorbents, that is, whether it was chemisorption or physisorption. Since the $\Delta G°$ values are in the range of −20 to 0 kJ mol^{-1} and the $\Delta H°$ values are in between –2 and –30 kJ mol^{-1}, it can be concluded that the physisorption is the predominant mechanism in the elimination of Cr(VI) ions [2,50].

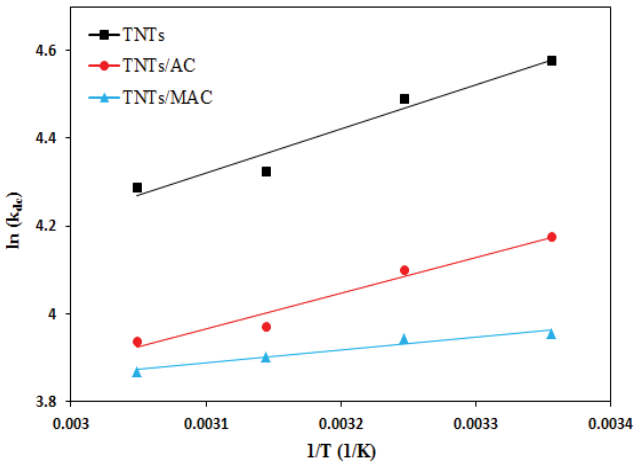

Fig. 12. Thermodynamic plot for the adsorption of Cr(VI) onto various nanoadsorbents.

4. Conclusion

In this study, the adsorption performance of ternary TNTs/MAC nanocomposite was investigated in the removal of Cr(VI) from wastewater. For this purpose, after characterization of nanoadsorbents, the batch adsorption experiments were carried out as a function of solution pH, adsorbent dosage, initial Cr(VI) concentration, contact time, and adsorption temperature. The EDS and FTIR analysis revealed that the TNTs/MAC nanocomposites mainly consisted of Ti, O, Na, C, and Fe atoms. Also the BET analysis indicated that MAC augments the surface attractive forces of TNTs to forming larger mesoporous pores (0.46 cm^3 g^{-1} pore volume). Experiments results showed the efficiency of adsorption removal of Cr(VI) has a close relationship with the solution pH, adsorbent dosage, and temperature. The maximum adsorption capacity of Cr(VI) onto TNTs/MAC nanocomposites was achieved at pH = 2, TNTs/MAC adsorbent dose of 0.3 g, contact time of 120 min, temperature of 298.15 K, and initial concentration of 50 mg L^{-1}. The kinetics data well followed the pseudo-second-order model, and the intra-particle diffusion model implied that overall process of adsorption was simultaneously controlled by boundary layer diffusion and intra-particle diffusion. In the meantime, the equilibrium data fitted well to the Langmuir model with a correlation coefficient greater than 0.99. The D-R model implied that the Cr(VI) adsorption onto TNTs/MAC nanocomposites is mainly physical adsorption. Furthermore, the thermodynamic variables and isotherm parameters indicated that adsorption of Cr(VI) is spontaneous, exothermal, favorable, and practical. The developed TNTs/MAC nanocomposites not only has demonstrated higher adsorption efficiency and fast kinetics but also have shown additional benefits such as ease of synthesis, easy recovery, cost-effectiveness, the absence of secondary pollutants and environmental friendliness. Hence it can be concluded to be a promising advanced nanoadsorbent in environmental pollution cleanup.

Acknowledgment

The authors would like to acknowledge the College of Engineering, University of Tehran for their esteemed financial support.

Table 4
Thermodynamic parameters for the adsorption of Cr(VI) onto different nanoadsorbents

Adsorbent	$\Delta G°$ (kJ mol^{-1})				$\Delta H°$ (kJ mol^{-1})	$\Delta S°$ (kJ mol^{-1} K^{-1})
	Temperature (K)					
	298.15	308.15	318.15	328.15		
TNTs	–9.80	–10.10	–10.31	–10.55	–2.46	0.025
TNTs/AC	–10.34	–10.49	–10.50	–10.73	–6.85	0.012
TNTs/MAC	–11.34	–11.55	–11.44	–11.70	–8.40	0.010

References

[1] M.O. Borna, M. Pirsaheb, M.V. Niri, R.K. Mashizie, B. Kakavandi, M.R. Zare, A. Asadi, Batch and column studies for the adsorption of chromium(VI) on low-cost Hibiscus cannabinus kenaf, a green adsorbent, J. Taiwan Inst. Chem. Eng., 68 (2016) 80–89.

[2] G. Ren, X. Wang, P. Huang, B. Zhong, Z. Zhang, L. Yang, X. Yang, Chromium (VI) adsorption from wastewater using porous magnetite nanoparticles prepared from titanium residue by a novel solid-phase reduction method, Sci. Total Environ., 607–608 (2017) 900–910.

[3] A.A. Yakout, H.M. Albishri, Solvo-thermal synthesis, characterization of aluminon-functionalized magnetic nanoparticles and investigation of its adsorption performance for Cr(VI) and Cr(III), J. Taiwan Inst. Chem. Eng., 55 (2015) 180–188.

[4] K. Zhang, H. Li, X. Xu, H. Yu, Synthesis of reduced graphene oxide/NiO nanocomposites for the removal of Cr(VI) from aqueous water by adsorption, Microporous Mesoporous Mater., 255 (2018) 7–14.

[5] L. Alidokht, A. Khataee, A. Reyhanitabar, S. Oustan, Reductive removal of Cr(VI) by starch-stabilized Fe^0 nanoparticles in aqueous solution, Desalination, 270 (2011) 105–110.

[6] N. Saranya, E. Nakeeran, M.S.G. Nandagopal, N. Selvaraju, Optimization of adsorption process parameters by response surface methodology for hexavalent chromium removal from aqueous solutions using Annona reticulata Linn peel microparticles, Water Sci. Technol., 75 (2017) 2094–2107.

[7] R.S. Moakhar, G.K.L. Goh, A. Dolati, M. Ghorbani, Sunlight-driven photoelectrochemical sensor for direct determination of hexavalent chromium based on Au decorated rutile TiO_2 nanorods, Appl. Catal., B, 201 (2017) 411–418.

[8] Ş. Parlayıcı, A. Yar, A. Avcı, E. Pehlivan, Removal of hexavalent chromium using polyacrylonitrile/titanium dioxide nanofiber membrane, Desal. Wat. Treat., 57 (2015) 16177–16183.

[9] N. Saranya, A. Ajmani, V. Sivasubramanian, N. Selvaraju, Hexavalent chromium removal from simulated and real effluents using *Artocarpus heterophyllus* peel biosorbent - Batch and continuous studies, J. Mol. Liq., 265 (2018) 779–790.

[10] S. Hosseini, S. Pourmortazavi, K. Gholivand, Spectrophotometric determination of chlorate ions in drinking water, Desalination, 245 (2009) 298–305.

[11] C. Liu, R.-N. Jin, X.-K. Ouyang, Y.-G. Wang, Adsorption behavior of carboxylated cellulose nanocrystal—polyethyleneimine composite for removal of Cr(VI) ions, Appl. Surf. Sci., 408 (2017) 77–87.

[12] A.S.K. Kumar, S.-J. Jiang, W.-L. Tseng, Effective adsorption of chromium(vi)/Cr(iii) from aqueous solution using ionic liquid functionalized multiwalled carbon nanotubes as a super sorbent, J. Mater. Chem. A, 3 (2015) 7044–7057.

[13] S. Rangabhashiyam, N. Anu, N. Selvaraju, Equilibrium and kinetic modeling of chromium(VI) removal from aqueous solution by a novel biosorbent, Res. J. Chem. Environ., 18 (2014) 30–36.

[14] S. Rangabhashiyam, E. Suganya, A.V. Lity, N. Selvaraju, Equilibrium and kinetics studies of hexavalent chromium biosorption on a novel green macroalgae *Enteromorpha* sp., Res. Chem. Intermed., 42 (2015) 1275–1294.

[15] S. Parlayici, V. Eskizeybek, A. Avcı, E. Pehlivan, Removal of chromium (VI) using activated carbon-supported-functionalized carbon nanotubes, J. Nanostructure Chem., 5 (2015) 255–263.

[16] N. Nasseh, L. Taghavi, B. Barikbin, A.R. Harifi-Mood, The removal of Cr(VI) from aqueous solution by almond green hull waste material: kinetic and equilibrium studies, J. Water Reuse Desal., 7 (2016) 449–460.

[17] E. Nakkeeran, N. Saranya, M.G. Nandagopal, A. Santhiagu, N. Selvaraju, Hexavalent chromium removal from aqueous solutions by a novel powder prepared from Colocasia esculenta leaves, Int. J. Phytorem., 18 (2016) 812–821.

[18] E. Nakkeeran, S. Rangabhashiyam, M.G. Nandagopal, N. Selvaraju, Removal of Cr(VI) from aqueous solution using *Strychnos nux-vomica* shell as an adsorbent, Desal. Wat. Treat., 57 (2016) 23951–23964.

[19] A. Gaffer, A.A.A. Kahlawy, D. Aman, Magnetic zeolite-natural polymer composite for adsorption of chromium (VI), Egypt. J. Pet., 26 (2017) 995–999.

[20] L. Niazi, A. Lashanizadegan, H. Sharififard, Chestnut oak shells activated carbon: Preparation, characterization and application for Cr (VI) removal from dilute aqueous solutions, J. Cleaner Prod., 185 (2018) 554–561.

[21] M. Rai, G. Shahi, V. Meena, R. Meena, S. Chakraborty, R. Singh, B. Rai, Removal of hexavalent chromium Cr (VI) using activated carbon prepared from mango kernel activated with H_3PO_4, Resour.-Effic. Technol., 2 (2016) S63–S70.

[22] U.K. Sahu, S.S. Mahapatra, R.K. Patel, Synthesis and characterization of an eco-friendly composite of jute fiber and Fe_2O_3 nanoparticles and its application as an adsorbent for removal of As(V) from water, J. Mol. Liq., 237 (2017) 313–321.

[23] J. Zhu, H. Gu, J. Guo, M. Chen, H. Wei, Z. Luo, H.A. Colorado, N. Yerra, D. Ding, T.C. Ho, N. Haldolaarachchige, J. Hopper, D.P. Young, Z. Guo, S. Wei, Mesoporous magnetic carbon nanocomposite fabrics for highly efficient Cr(vi) removal, J. Mater. Chem. A, 2 (2014) 2256–2265.

[24] B. Qiu, Y. Wang, D. Sun, Q. Wang, X. Zhang, B.L. Weeks, R. Oconnor, X. Huang, S. Wei, Z. Guo, Cr(VI) removal by magnetic carbon nanocomposites derived from cellulose at different carbonization temperatures, J. Mater. Chem. A, 3 (2015) 9817–9825.

[25] M. Fatehi, J. Shayegan, M. Zabihi, I. Goodarznia, Functionalized magnetic nanoparticles supported on activated carbon for adsorption of Pb(II) and Cr(VI) ions from saline solutions, J. Environ. Chem. Eng., 5 (2017) 1754–1762.

[26] S. Srivastava, S.B. Agrawal, M.K. Mondal, Synthesis, characterization and application of *Lagerstroemia speciosa* embedded magnetic nanoparticle for Cr(VI) adsorption from aqueous solution, J. Environ. Sci., 55 (2017) 283–293.

[27] S.A. Elfeky, S.E. Mahmoud, A.F. Youssef, Applications of CTAB modified magnetic nanoparticles for removal of chromium (VI) from contaminated water, J. Adv. Res., 8 (2017) 435–443.

[28] B.Y.L. Tan, M.H. Tai, J. Juay, Z. Liu, D. Sun, A study on the performance of self-cleaning oil–water separation membrane formed by various TiO_2 nanostructures, Sep. Purif. Technol., 156 (2015) 942–951.

[29] X. Shen, Q. Wang, Q. Wu, S. Guo, Z. Zhang, Z. Sun, B. Liu, Z. Wang, B. Zhao, W. Ding, CoB supported on Ag-activated TiO_2 as a highly active catalyst for hydrolysis of alkaline $NaBH_4$ solution, Energy, 90 (2015) 464–474.

[30] Y. Ma, X. Li, Y. Zhang, L. Chen, J. Wu, D. Gao, J. Bi, G. Fan, Ruthenium nanoparticles supported on TiO_2 (B) nanotubes: effective catalysts in hydrogen evolution from the hydrolysis of ammonia borane, J. Alloys Compd., 708 (2017) 270–277.

[31] B. Hu, G. Chen, C. Jin, J. Hu, C. Huang, J. Sheng, G. Sheng, J. Ma, Y. Huang, Macroscopic and spectroscopic studies of the enhanced scavenging of Cr(VI) and Se(VI) from water by titanate nanotube anchored nanoscale zero-valent iron, J. Hazard. Mater., 336 (2017) 214–221.

[32] B. Buchholcz, K. Plank, M. Mohai, Á. Kukovecz, J. Kiss, I. Bertóti, Z. Kónya, Morphology conserving high efficiency nitrogen doping of titanate nanotubes by NH_3 plasma, Top. Catal., 61 (2018) 1263–1273.

[33] R. Ma, X. Wang, J. Huang, J. Song, J. Zhang, X. Wang, Photocatalytic degradation of salicylic acid with magnetic activated carbon-supported F-N codoped TiO_2 under visible light, Vacuum, 141 (2017) 157–165.

[34] J.V. Pasikhani, N. Gilani, A.E. Pirbazari, The effect of the anodization voltage on the geometrical characteristics and photocatalytic activity of TiO_2 nanotube arrays, Nano-Struct. Nano-Objects, 8 (2016) 7–14.

[35] J.V. Pasikhani, N. Gilani, A.E. Pirbazari, The correlation between structural properties, geometrical features, and photoactivity of freestanding TiO_2 nanotubes in comparative degradation of 2,4-dichlorophenol and methylene blue, Mater. Res. Express, 5 (2018) 025016.

[36] J.V. Pasikhani, N. Gilani, A.E. Pirbazari, Improvement the wastewater purification by TiO_2 nanotube arrays: the effect of etching-step on the photo-generated charge carriers and photocatalytic activity of anodic TiO_2 nanotubes, Solid State Sci., 84 (2018) 57–74.

[37] C. Chen, Q. Liu, S. Gao, K. Li, H. Xu, Z. Lou, B. Huang, Y. Dai, Celastrol-modified TiO_2 nanoparticles: effects of celastrol on the particle size and visible-light photocatalytic activity, RSC Adv., 4 (2014) 12098–12104.
[38] B.N. Dorakumbura, R.E. Boseley, T. Becker, D.E. Martin, A. Richter, M.J. Tobin, W.V. Bronswjik, J. Vongsvivut, M.J. Hackett, S.W. Lewis, Revealing the spatial distribution of chemical species within latent fingermarks using vibrational spectroscopy, Analyst, 143 (2018) 4027–4039.
[39] Ratnawati, J. Gunlazuardi, E.L. Dewi, Slamet, Effect of $NaBF_4$ addition on the anodic synthesis of TiO_2 nanotube arrays photocatalyst for production of hydrogen from glycerol–water solution, Int. J. Hydrogen Energy, 39 (2014) 16927–16935.
[40] D. Tsiourvas, A. Tsetsekou, M. Arkas, S. Diplas, E. Mastrogianni, Covalent attachment of a bioactive hyperbranched polymeric layer to titanium surface for the biomimetic growth of calcium phosphates, J. Mater. Sci. - Mater. Med., 22 (2010) 85–96.
[41] M. Thommes, K. Kaneko, A.V. Neimark, J.P. Olivier, F. Rodriguez-Reinoso, J. Rouquerol, K.S. Sing, Physisorption of gases, with special reference to the evaluation of surface area and pore size distribution (IUPAC Technical Report), Pure Appl. Chem., 87 (2015) 1051–1069.
[42] Y. Zhang, D. Shao, J. Yan, X. Jia, Y. Li, P. Yu, T. Zhang, The pore size distribution and its relationship with shale gas capacity in organic-rich mudstone of Wufeng-Longmaxi Formations, Sichuan Basin, China, J. Nat. Gas Geosci., 1 (2016) 213–220.
[43] L. Zhang, Y. Zhang, Adsorption characteristics of hexavalent chromium on HCB/TiO_2, Appl. Surf. Sci., 316 (2014) 649–656.
[44] H. Shekari, M. Sayadi, M. Rezaei, A. Allahresani, Synthesis of nickel ferrite/titanium oxide magnetic nanocomposite and its use to remove hexavalent chromium from aqueous solutions, Surf. Interfaces, 8 (2017) 199–205.
[45] X. Zhou, G. Jing, B. Lv, Z. Zhou, R. Zhu, Highly efficient removal of chromium(VI) by Fe/Ni bimetallic nanoparticles in an ultrasound-assisted system, Chemosphere, 160 (2016) 332–341.
[46] M. Arshadi, F. Mousavinia, A. Khalafi-Nezhad, H. Firouzabadi, A. Abbaspourrad, Adsorption of mercury ions from wastewater by a hyperbranched and multi-functionalized dendrimer modified mixed-oxides nanoparticles, J. Colloid Interface Sci., 505 (2017) 293–306.
[47] M. Dinari, A. Haghighi, Surface modification of TiO_2 nanoparticle by three dimensional silane coupling agent and preparation of polyamide/modified- TiO_2 nanocomposites for removal of Cr (VI) from aqueous solutions, Prog. Org. Coat., 110 (2017) 24–34.
[48] K. Bhattacharya, D. Parasar, B. Mondal, P. Deb, Mesoporous magnetic secondary nanostructures as versatile adsorbent for efficient scavenging of heavy metals, Sci. Rep., 5 (2015) 1–9.
[49] W. Jiang, M. Pelaez, D.D. Dionysiou, M.H. Entezari, D. Tsoutsou, K. O'Shea, Chromium(VI) removal by maghemite nanoparticles, Chem. Eng. J., 222 (2013) 527–533.
[50] A. Mohamed, W. Nasser, T. Osman, M. Toprak, M. Muhammed, A. Uheida, Removal of chromium (VI) from aqueous solutions using surface modified composite nanofibers, J. Colloid Interface Sci., 505 (2017) 682–691.